INSTITUT DE FRANCE
Académie des sciences

Comptes Rendus

Géoscience

Sciences de la Planète

Nicolas Tribovillard, Viviane Bout-Roumazeilles, Romain Abraham, Sandra Ventalon, Marion Delattre and François Baudin

The contrasting origins of glauconite in the shallow marine environment highlight this mineral as a marker of paleoenvironmental conditions

Volume 355, Special Issue S2 (2023), p. 213-228

Online since: 13 December 2022

Part of Special Issue: Tribute to Jean Dercourt

Guest editors: François Baudin (Institut des Sciences de la Terre - Paris (ISTeP), Sorbonne Université), Éric Calais (École normale supérieure, Département de Géosciences, Paris) and François Chabaux (Institut Terre Environnement de Strasbourg (UMR 7063-Unistra-CNRS-ENGEES), Université de Strasbourg)

https://doi.org/10.5802/crgeos.170

The Comptes Rendus. Géoscience — Sciences de la Planète *are a member of the Mersenne Center for open scientific publishing*
www.centre-mersenne.org — e-ISSN : 1778-7025

Comptes Rendus
Géoscience — Sciences de la Planète
2023, Vol. 355, Special Issue S2, p. 213-228
https://doi.org/10.5802/crgeos.170

Research article

Tribute to Jean Dercourt

The contrasting origins of glauconite in the shallow marine environment highlight this mineral as a marker of paleoenvironmental conditions

Nicolas Tribovillard [*, a], Viviane Bout-Roumazeilles [a], Romain Abraham [a], Sandra Ventalon [a], Marion Delattre [a] and François Baudin [b]

[a] Université de Lille, UMR 8187 LOG – Laboratoire d'Océanologie et de Géosciences, Univ. Lille, CNRS, Univ. Littoral Côte d'Opale, IRD, 59000 Lille, France

[b] Sorbonne Université - CNRS, Institut des Sciences de la Terre de Paris, UMR ISTeP 7193, 75005 Paris, France

E-mails: nicolas.tribovillard@univ-lille.fr (N. Tribovillard), viviane.roumazeilles@univ-lille.fr (V. Bout-Roumazeilles), romain.abraham@univ-lille.fr (R. Abraham), sandra.ventalon@univ-lille.fr (S. Ventalon), marion.delattre@univ-lille.fr (M. Delattre), francois.baudin@sorbonne-universite.fr (F. Baudin)

Abstract. Glauconite is an authigenic mineral reputed to form during long-lasting contact between a nucleus (a pre-existing phyllosilicate) and seawater. This protracted contact makes it possible to subtract the ions necessary for the construction of the neoformed phyllosilicate, here, glauconite (a mineral very close to an illite, rich in K and Fe). As a result, glauconite is often associated with sediments deposited in a transgressive context with a strong slowdown in the rate of sedimentation and a relatively large water layer thickness. This is the case of the Cenomanian chalk of Boulonnais (north of France). Being chemically and physically resistant, glauconite is a mineral that is often reworked, like quartz grains. This is frequently the case of the Jurassic deposits of the Boulonnais, where glauconite, almost ubiquitous, either in traces or in significant proportions of the sediments, presents a grain size sorting attesting to its transport and reworking. However, these Jurassic deposits are shallow (shoreface, upper offshore), which supports the idea that the "glauconite factory" was itself in the shallow areas of the Boulonnais. The only identified Jurassic facies of the Boulonnais where glauconite is both relatively abundant, large in size and unsorted (non reworked) are oyster reefs that formed at the outlet of cold seeps linked to a late-Jurassic synsedimentary tectonic (Kimmeridgian, Tithonian). Our work makes it possible to hypothesize that isolated oyster reefs were environments combining the redox conditions and in contact with seawater favoring the authigenic formation of glauconite. The weakly reducing conditions necessary for the formation of glauconite here are attested by the contents of metallic trace elements sensitive to redox conditions (vanadium, germanium, arsenic, in this case). Our work thus adds a new element to the understanding of the mechanisms of formation of glauconite in shallow environments.

Keywords. Jurassic, Cretaceous, Boulonnais, Oyster reefs, Redox-proxies.

Manuscript received 26 August 2022, revised 20 September 2022, accepted 5 October 2022.

1. Introduction

Glauconite and other green minerals (berthierine, odinite, etc.) are authigenic sedimentary minerals

* Corresponding author.

that form slowly at the sediment–water interface or in its immediate vicinity, as is known, especially since the work of Odin and Matter [1981]. The formation and growth of these phyllosilicates require protracted exchanges between a nucleus (usually a pre-existing clay mineral) and seawater. Glauconite is a mineral close to an illite, rich in potassium and iron, present in both Fe^{2+} and Fe^{3+} forms simultaneously. Its formation therefore requires weakly reducing conditions allowing the co-existence of ferrous ions and ferric ions. A case favoring the formation of glauconite may meet the following conditions [Chamley, 2001, Meunier and El Albani, 2007, Velde, 2014, Banerjee et al., 2016a,b, Bennett and Canfield, 2020]: (1) the presence of organic matter is crucial, because its decomposition favors the development of oxygen-poor conditions and, therefore, reducing micro-milieus (fecal pellets, interior of foraminifera tests). Simultaneously, organic decay allows the release of iron initially bound to organic matter. (2) The oxidation of pre-existing pyrite also makes iron available, although this element is usually not abundant in dissolved form in seawater. (3) Finally, a long period of exchange with seawater allows the capture and incorporation of K^+ ion into the crystal lattice during neoformation (authigenic growth). This mineral is therefore able to undergo and record the paleoenvironmental conditions that prevailed at the sediment–water interface (or at shallow depth beneath it) during its authigenic growth. This character of redox marker is central to the study proposed here. This character has very rarely been studied on the basis of the content of trace elements sensitive to redox conditions [Tribovillard et al., 2021] because, to the best of our knowledge, previous studies focused on the content of major elements [e.g., Baldermann et al., 2022, and reference therein]. This work therefore represents an unprecedented approach to understanding the formation of this mineral that is relatively ubiquitous in time and space on the scale of geological ages. This mineral has been extensively studied but is not fully understood, although a lot is known. Due to its mode of formation, glauconite is reputed to originate mainly from offshore areas of the continental shelf where sedimentation rates can be (extremely) low. This makes it a tool for identifying episodes of marine transgression in sequence stratigraphy patterns [e.g. Amorosi and Centineo, 2000, Hesselbo and Huggett, 2001, Banerjee et al., 2022]. Simultaneously, many studies have shown that glauconite could also appear in proximal environments, possibly estuarine or lagoonal-lacustrine [El Albani et al., 2005].

In the Mesozoic of Boulonnais (Northernmost France; Figure 1), glauconite is very often mentioned in the Jurassic deposits as well as under the base of the Chalk formation (glauconious sandstone of the Aptian-Albian), and in the lower part of the Chalk of Cenomanian age [Mansy et al., 2007]. If the Cenomanian glauconite is interpreted as having formed contemporaneously with the chalk deposition [Amorosi and Centineo, 2000], in connection with the great transgression of the Upper Cretaceous and the concomitant decrease in sedimentation rates (synsedimentary glauconite), the glauconites of the Aptian-Albian sandstones and those of the Jurassic formations studied here show a grain size sorting attesting to their reworking (unpublished results included in this article). Thus, is it possible to consider that these reworked glauconites were initially formed in shallow environments, perhaps estuarine ones? Finally, the Jurassic deposits rich in reworked glauconite being also rich in small oyster shells (*nanogyra*) put in place during storms, the question arises as to whether the sources of glauconite could be the oyster reefs identified in the Kimmeridgian-Tithonian Argiles de Châtillon Formation [Hatem et al., 2014]. Thus, the questions addressed here are: (1) Are oyster reefs the glauconite factory fueling storm deposits? (2) Given that the Upper Jurassic formations were deposited under conditions that were more reducing and more favorable to the accumulation of organic matter than those that prevailed during the deposit of the Cenomanian chalk, it is wondered whether the glauconites—possible markers of the conditions at the sediment–water interface—are enriched in redox-sensitive trace elements in Jurassic deposits compared to what is observed in the chalk.

2. Geological background

2.1. *Stratigraphic framework*

From the much detailed explanatory note of the geological map of Marquise [Mansy et al., 2007], the stratigraphic framework of this study (Figure 1) can be sketched as follows. The study area extends from Cap de la Crèche (south of the town of Wimereux)

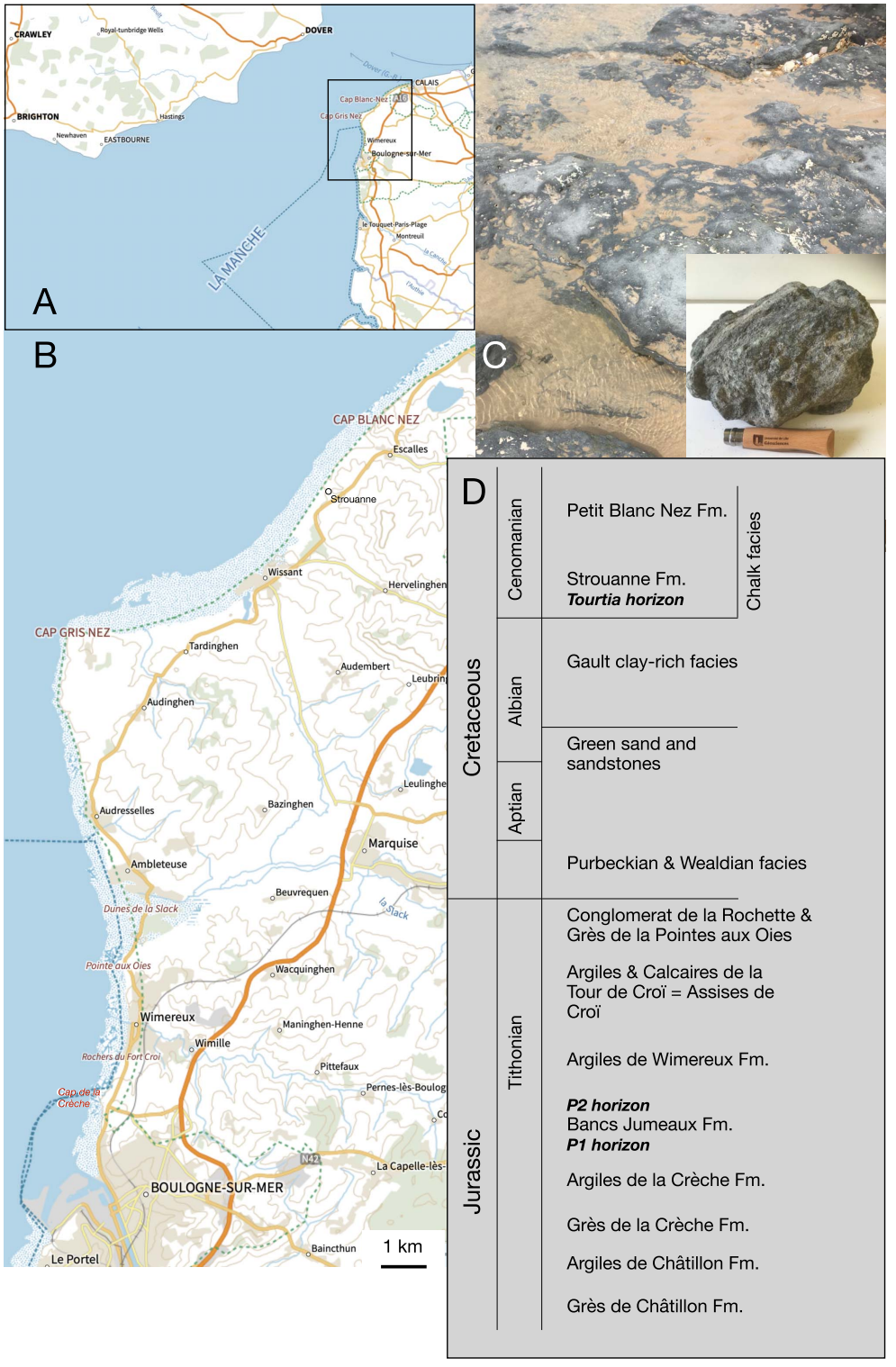

Figure 1. (A) Location of the studied zone within the English Channel. (B) Detail of the coastline of the Boulonnais with the sampling sites mentioned. (C) View of the glauconite-rich basal level of the Cenomanian chalk, the so-called Tourtia level. (D) Stratigraphy of the Upper Jurassic-Cretaceous formations of the Boulonnais.

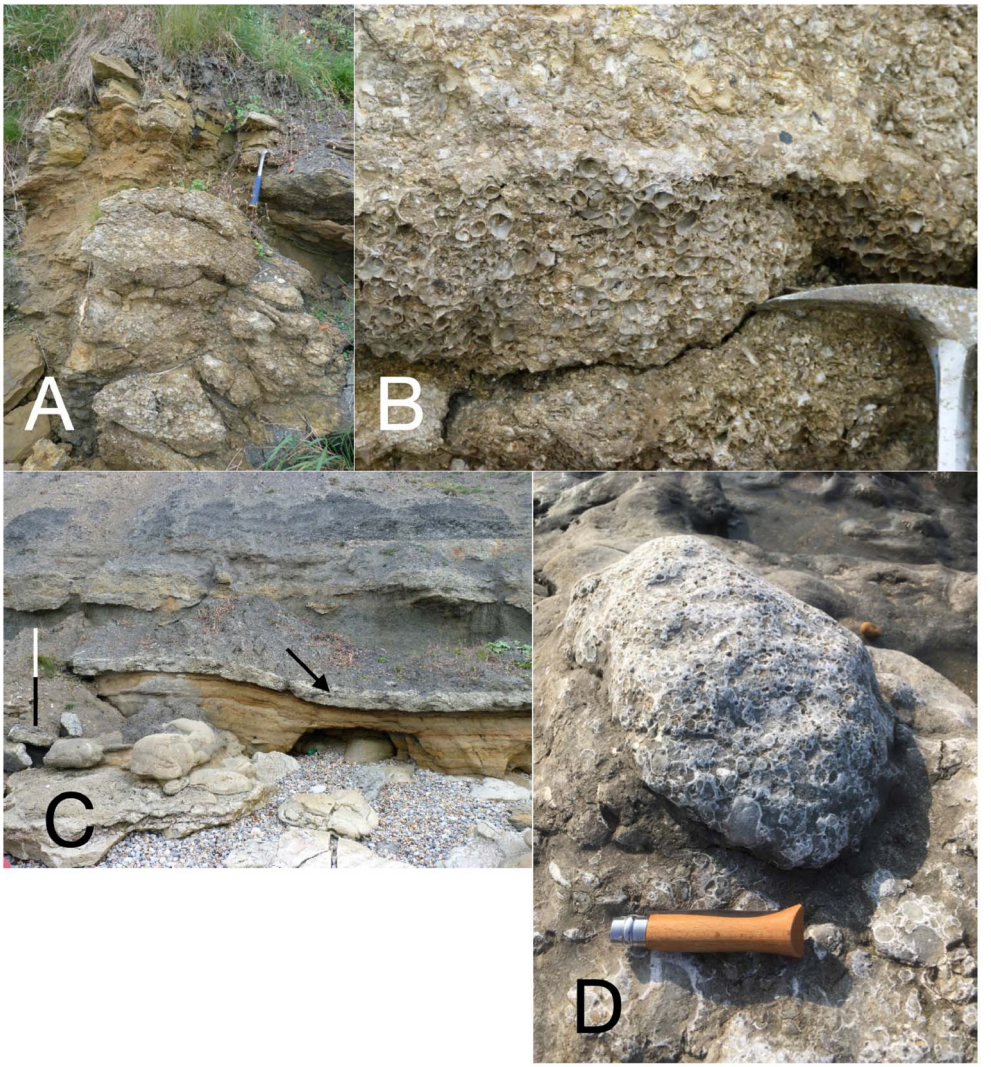

Figure 2. (A) An oyster patch reef on the beach called "La Sirène" at Cap Gris-Nez. (B) Close up view of the oyster reef. (C) The carbonate bed (arrow) separating the Grès de Châtillon Fm. (below) and the Argile de Châtillon Fm. (above). The scale bar is 2 m long. This bed, called the "Boundary Bed", is colonized by sparse, small dimension, patch reefs (D).

to Cap Blanc Nez (Figure 1) and presents outcrops ranging in age from the Tithonian to the Cenomanian. The geological formations studied in this work start with the upper part of the Grès de Châtillon Formation (Fm.), deposited in a very shallow context. These sandstones are overlain by dark marly formations indicating a greater water depth: the Argiles de Châtillon Fm. (Figure 2). The transition from the Grès de Châtillon to the Argiles de Châtillon is marked by a specific bed containing small oyster path reefs [the so-called Boundary Bed of Hatem et al., 2016; Figure 2]. The top of the Argiles de Châtillon corresponds to the return to shallow-depth conditions of deposition, with the presence of the Grès de la Crèche Fm. (Supplementary Figure S1). Above, come two marly formations, the Argiles de la Crèche and the Argiles de Wimereux formations. These two formations are separated by a meter-scale alternation of diagenetic limestone beds and marly interbeds: the Bancs Jumeaux Fm. [Tribovillard

et al., 2012]. This formation is marked at its base and top by two discontinuity surfaces rich in phosphate debris and glauconite, the levels P1 and P2, respectively (Supplementary Figure S2). The end of the Jurassic marine-deposition episode is represented by an alternation of limestone beds and marly interbeds, both facies being glauconious (the Formation des Argiles et Calcaires of the Tour de Croï, a.k.a. Assises de Croï), which are overlain by shallow, detrital deposits showing conglomerates and sandstones with storm structures (Conglomérat de la Rochette and Grès de la Pointe aux Oies; Supplementary Figure S3). The regression that characterizes the transition from the Jurassic to the Cretaceous is echoed by freshwater carbonate stromatolites (Purbeckian facies) overlain by continental deposits (Wealdian facies). The Cretaceous transgression will be marked by the deposition of green sands and sandstones from Aptian to Lower Albian age. The middle and upper Albian is made of clay and marl deposits, sometimes glauconious (the so-called Argiles du Gault, a.k.a. the Saint-Pô and Lottinghen formations). The Cenomanian witnessed the establishment of conditions conducive to the deposition of chalk, which lasted until the end of the Cretaceous. The initial meters of chalk (the Strouanne Fm.) are very rich in glauconite. The basal level of this formation, called Tourtia, is very dark, and remarkably abundant with glauconite (Figure 1). This conspicuous level has a regional extension. The Cenomanian continues with the clayey chalk of the Petit Blanc Nez Fm.; glauconite is only present in small quantities, restricted to certain horizons. This brief presentation is illustrated in Supplementary Figure S4.

2.2. *Short presentation of glauconite*

Glauconite is a hydrous phyllosilicate rich in iron and potassium with the formula: $(K,Na)(Fe^{3+},Fe^{2+},Al,Mg)_2\ 3[Si_3(Si,Al)O_{10}](OH)_2,4H_2O$ is a mineral generally interpreted to be of diagenetic origin [Odin and Matter, 1981, Amorosi, 1995, El Albani et al., 2005, Banerjee et al., 2016a,b, López-Quirós et al., 2020]. Some conditions are commonly invoked to account for the formation of glauconite at, or close to, the sediment–water interface: reduced sedimentation rates allowing long-lasting availability of dissolved cations, together with oxygen-depleted, mildly reducing, conditions [Odin and Matter, 1981, Meunier and El Albani, 2007, Choudhury et al., 2021, Huggett, 2021]. Glauconite usually appears as lobate grains (pellets), with frequent cracked surfaces [Boyer et al., 1977, Bayliss and Syvitski, 1982]. Along with its K_2O concentration, the morphologic characteristics of glauconite are used as criteria to estimate the duration of the authigenic formation of this mineral [Velde, 2014]. Finally, glauconite is commonly used as a tool for reconstructing sea-level variations [e.g., Banerjee et al., 2008, 2016a,b, Amorosi and Centineo, 2000, Hesselbo and Huggett, 2001, Huggett et al., 2017].

3. Materials and methods

Table 1 summarizes the sampling conducted for this study. We completed the chalk sampling [Tribovillard et al., 2021] with samples from the Tourtia level, very rich in glauconite, taken from two outcrops between Strouanne and Cap Blanc Nez (Figure 1). To examine transgressive episodes of the Upper Jurassic, in order to compare them to the transgression of the base of the Cenomanian chalk, we sampled the transition from sandstone deposited in a very shallow environment to marls that are first sandy/silty and then progressively more clayey upward: the transition from the Grès de Châtillon Fm. to the Argiles de Châtillon Fm. (Figure 2) and the one from the Grès de la Crèche Fm. to the Argiles de la Crèche Fm. (Supplementary Figure S1). In the Argiles de Châtillon, we studied in particular the oyster reefs at the base of the formation (Figure 2), and the levels of tempestites showing a lumachel (a.k.a. coquina bed) facies where the rock is only made of compressed shells of small oysters [dominantly *nanogyra nana, accessorily n. virgula*; Fürsich and Oschmann, 1986; Figure 3]. Several of these tempestites have been examined, in particular the one accompanying the Kimmeridgian/Tithonian boundary that separates the formation of the Argiles de Châtillon in two parts, as well as lenticular lumachels scattered in the claystone level located immediately below the Kimmeridgian-Tithonian boundary. We have also examined shell-rich levels in which oyster shells are abundant but not exclusive as they are in lumachels: levels P1 and P2 of the Bancs Jumeaux Fm. (Supplementary Figure S2) and three levels of

Table 1. Recapitulation of the sampling site along the Boulonnais coastline

Age	Geological formations	Sampled levels	Location (see Figure 1)
Cretaceous	Cenomanian Chalk	Glauconious chalk at the lowermost part of the formation	Beach between Strouanne and Cap Blanc Nez
	Aptian-Albian sandstones	Dark-colored sandstones visible at low tide	Strouanne beach
Jurassic	Assise de Croï	Two shell-rich carbonate levels and one marly interbed	Pointe aux Oies (N Wimereux)
	Bancs Jumeaux	P1 and P2 levels and each of the marly interbeds	Pointe aux Oies (N Wimereux)
	Argiles de la Crèche	Silty marls at the very base of the formation	Rochers du Fort Croï (S Wimereux)
	Grès de la Crèche	Two green-colored marly interbeds of the topmost part of the formation (Tithonian)	Rochers du Fort Croï (S Wimereux)
	Argiles de Châtillon	Coquina beds of the Kimmeridgian-Tithonian boundary and immediately below it	North of Audresselles (Cran du Noirda)
	Argiles de Châtillon	Silty marls at the base of the formation evolving to black shales (Kimmeridgian)	North of Audresselles (Cran du Noirda)
	Argiles de Châtillon	Oyster patch reefs at the base of the formation (the Boundary Bed, Kimmerdigian)	North of Audresselles (Cran du Noirda) and Cap Gris Nez (plage de la Sirène)

See Figure 1 for their location.

the Assises de Croï Fm.: two limestone levels and a marly inter-bed (Supplementary Figure S5).

The glauconite grains were isolated through the following protocol. Samples were digested with HCl to dissolve the carbonate phases before being rinsed. Several rinses were carried out with the necessary time for minerals heavier than clays to settle and to be removed with the supernatant. This operation was repeated at least 25 times, until the liquid kept limpid. What remained in the beakers was grains of glauconite and quartz (plus some accessory minerals and woody fragments). Glauconite was then separated from quartz using a Frantz magnetic separator. The grain size of the glauconite particles was studied using a laser beam-equipped analyzer Malvern MasterSizer [protocol described in Trentesaux et al., 2001]. The glauconite particles were imaged using a scanning electron microscope (SEM) equipped with a EDS-type analytical probe. The grains were also analysed by X-ray diffraction (XRD) to determine their mineralogy according to the standard protocol described in Bout-Roumazeilles et al. [1999] and Tribovillard et al. [2021]. XRD was carried out on both oriented mounts and non-oriented mounts to fully discriminate glauconite from illite. Lastly, the elemental composition (major and trace elements) of the glauconite grains was analysed at the CNRS analytical facility: the Rock and Mineral Analysis Service (SARM), in Vandoeuvre-les-Nancy [see details of the analytical protocol (ICP-OES and ICP-MS) in Carignan et al., 2004]. Some bulk-rock, coquina bed samples were analysed with a Thermo CHNS elemental analyser to determine the abundance of sulfur (pyrite) in this facies.

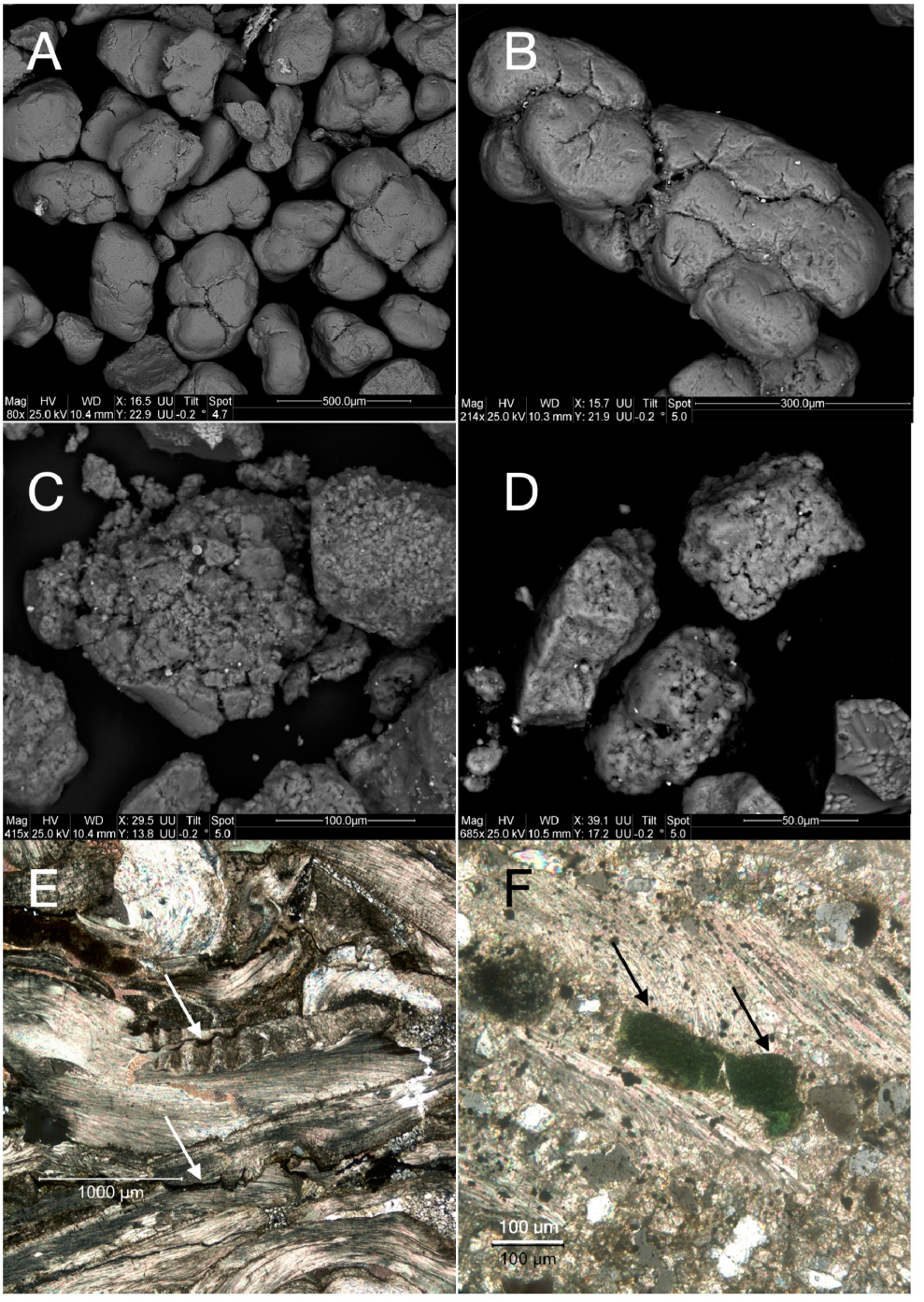

Figure 3. (A,B) Examples of glauconite grains from the oyster reefs. (C,D) Examples of glauconite grains contained in the coquina beds. Note their smaller dimensions and the marked corrosion. (E,F) Thin section observation of a coquina bed showing the dense packing of the oyster shells locally cemented with pyrite (E; white arrow) and containing glauconite grains (F; black arrows).

4. Results

Mineralogical analyses show that the green grains observed in this study are all glauconite. Tribovillard et al. [2021] had made this observation for chalk samples and it can be extended to all Jurassic and Aptian-Albian samples studied here. This seems to be a constant of the Mesozoic sedimentary deposits of the Boulonnais. Glauconite is almost omnipresent in our samples, but in very contrasting proportions. It has only been detected in quantities allowing its extraction and analysis in the chalk, the Aptian-Albian sandstones, the oyster reefs, the P1 and P2 levels, the Assises de Croï and the lumachels. In the later, glauconite is present but in variable amounts according to the samples, not always allowing grain size analysis (Figure 4 and Supplementary Figures S6–S8), even when rock samples of 500 g are studied. These lumachels are sometimes very rich in pyrite, seen in the form of cement (Figure 3) and not framboids. Their sulfur content can reach 28 wt%, which is considerable. Moreover, these rocks are very hard under the hammer and are difficult to fragment. It is observed that the richer the lumachels in pyritic cement, the less abundant the glauconite; the glauconite grains seen are of very small size and appear corroded when observed under the microscope (Figure 3).

In all the other samples studied, glauconite grains are systematically present but in insignificant quantities. The grain size analyzes of the samples rich in glauconite make it possible to distinguish two categories of samples, those where the grains of glauconite are poorly sorted (all the samples from the chalk and those from the oyster reefs) and those where the grains of glauconite are well sorted (all others; Figure 4 and Supplementary Figures S6–S8). The poorly sorted glauconite grains are also larger in size than the others. Regarding the samples from the Assises de Croï, where the glauconite is well sorted, the limestone levels show a mode at 78 µm and 65.5 µm, respectively, while the marly inter-bed shows a mode at 34 µm (Supplementary Figure S7).

In the samples where glauconite is well sorted, the grain size distribution of the quartz grains (isolated through magnetic separation) shows an even better sorting. See for instance the P1 and P2 samples or the Atian-Albian samples (Figure 4). Glauconite being usually a bit denser than quartz (2.40–2.95 g/cm^3

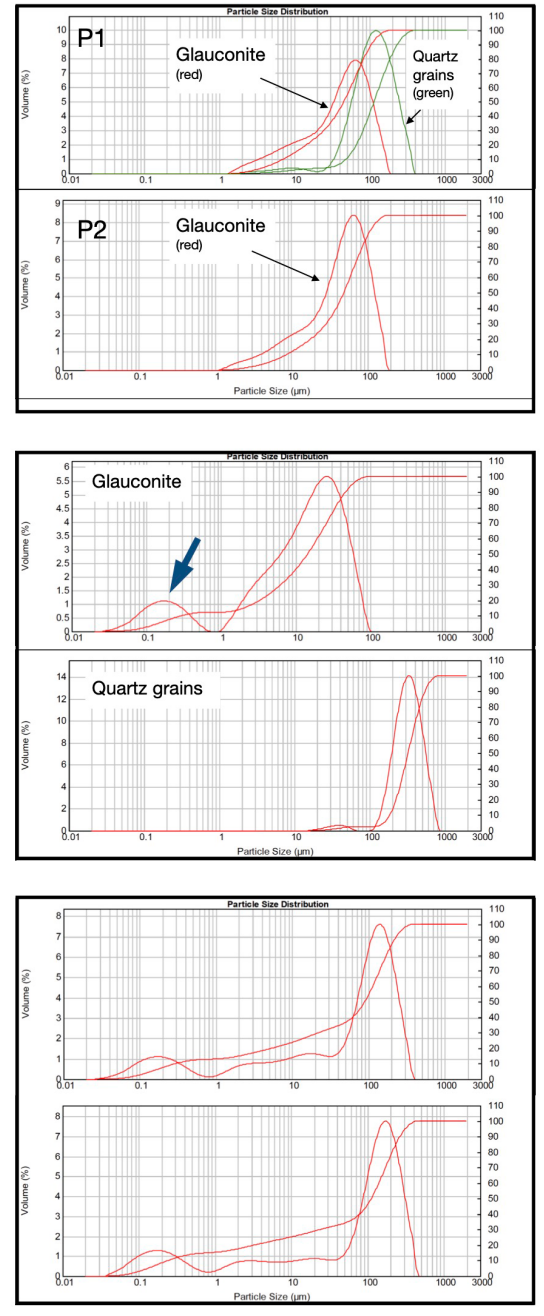

Figure 4. Illustrations of the grain size distribution patterns for glauconite and quartz grains of the P1 and P2 levels of the Bancs Jumeaux Fm., the Aptian-Albian sandstones and the Cenomanian chalk. The arrow points to a clay-sized fraction of glauconite probably released during grain wear induced by the measuring device.

Table 2. Chemical composition of 16 samples from various formations

Samples	As	Co	Cr	Cu	Ge	Ni	U	V	Zn	SiO2	Al2O3	Fe2O3	MnO	MgO	CaO	Na2O	K2O	TiO2	P2O5	LOI	Total
	µg/g	µg/g	µg/g	µg/g	µg/g	µg/g	µg/g	µg/g	µg/g	%	%	%	%	%	%	%	%	%	%	%	%
Cenomanian Chalk	5.87	25.9	115	3.6	5.0	53.1	0.15	96.2	55.5	50.82	7.81	20.1	< L.D.	4.1	0.31	0.02	8.21	0.05	< L.D.	7.61	98.86
Tourtia 1 Chalk base	5.55	25.3	110	< L.D.	4.7	49.4	0.10	86.8	46.8	52.52	7.54	19.37	< L.D.	3.82	0.30	0.02	7.85	0.06	< L.D.	7.45	98.92
Tourtia 2 Chalk base	5.83	25.0	118	< L.D.	5.0	46.7	0.13	90.5	51.6	51.61	7.46	20.15	< L.D.	3.84	0.31	< L.D.	8.3	0.05	< L.D.	7.35	98.80
ONM 1 Cenom Chalk	5.86	24.3	115	48.8	4.8	53.0	0.13	92.0	54.9	53.03	7.66	19.59	< L.D.	3.98	0.38	0.03	8.19	0.06	< L.D.	7.29	100.20
ONM 1 Cenom Chalk	6.8	33.3	109	28.8	4.8	64.6	0.09	92.4	50.0	52.45	7.95	19.46	< L.D.	4.18	0.31	0.03	8.39	0.04	< L.D.	7.39	100.20
ONM 1 Cenom Chalk	5.82	29.2	113	34.2	5.3	68.8	0.10	94.5	58.2	52.51	7.95	19.43	< L.D.	4.27	0.30	0.03	8.48	0.04	< L.D.	7.28	100.29
ONM 1 Cenom Chalk	6.9	25.4	125	5.4	5.1	52.6	0.15	95.8	54.3	52.31	7.63	20.28	< L.D.	3.97	0.34	0.02	8.25	0.05	< L.D.	7.43	100.28
Glauconious Sandstone 1	25.1	28.5	218	9.5	5.3	52.5	0.31	322	89.1	51.06	10.34	17.16	0.016	3.59	0.53	0.05	6.98	0.36	< L.D.	8.99	99.07
Assises de Croi 1	26.8	9.9	139	4.4	8.1	18.0	0.23	132	72.5	47.47	5.44	27.47	< L.D.	2.73	0.20	0.03	8.9	0.05	0.17	7.32	98.96
Assises de Croi 2	25.2	8.9	138	3.8	8.1	18.8	0.33	126	72.7	47.66	5.50	27.41	< L.D.	2.73	0.20	0.03	8.12	0.05	0.17	7.26	99.13
Bancs Jumeaux P1	28.4	14.7	302	13.1	8.1	22.8	0.85	150	74.9	49.39	7.34	22.97	0.017	2.42	0.31	0.08	7.6	0.24	0.27	8.99	99.07
Bancs Jumeaux P2	27.2	12.1	280	11.6	8.6	17.7	0.46	138	71.8	56.14	6.58	19.14	< L.D.	2.10	0.42	0.06	6.30	0.22	0.12	8.16	99.25
Oyster patch reef 1	26.9	10.0	138	4.3	8.1	18.0	0.13	131	72.0	47.74	5.45	27.74	< L.D.	2.37	0.19	0.03	8.90	0.06	0.18	7.23	99.89
Oyster patch reef 2	26.0	9.9	139	3.9	8.1	17.8	0.13	128	71.7	47.55	5.42	27.14	< L.D.	2.79	0.20	0.02	8.21	0.04	0.16	7.62	99.15
Oyster patch reef 3	26.1	29.5	267	23.0	5.3	60.2	0.68	327	99.0	50.89	10.10	16.76	0.021	3.52	0.58	0.06	6.78	0.73	0.13	9.7	98.64
Oyster patch reef 4	26.9	10.0	143	11.5	8.0	21.1	0.27	130	70.9	47.62	5.48	27.17	< L.D.	2.74	0.19	0.03	8.14	0.05	0.16	7.91	99.50

Blue: the Jurassic samples; green: the Cretaceous ones, Aptian-Albian glauconious sandstones and Cenomanian chalk.

versus 2.68 g/cm^3), the mode of the size distribution pattern expectedly shifts toward smaller particle sizes for glauconite compared to quartz. This shift does not preclude that glauconite and quartz have been deposited simultaneously. Regarding the sandstone-to-sandy claystone transition from the Grès de la Crèche to the overlying Argiles de la Crèche, i.e., formations where glauconite is not significantly present, a well-sorted distribution is observed for the carbonate-free fractions of the sediments. Incidentally, the fallacious green color observed for the marly interbeds of the Grès de la Crèche must be ascribed to the presence of green clays in the absence of glauconite, as evidenced through XRD analysis.

Finally, the particle size analysis of the poorly sorted samples using the Malvern apparatus shows the presence of particles of micrometer size whereas the extraction protocol should have resulted in their elimination (arrow on Figure 3 illustrating the grain size distribution). After separation and analysis (XRD) of this very fine fraction, it appears to be made of glauconite. We believe that these very fine particles are released during the analysis itself, by wear of the grains circulating into the pipes of the apparatus (see discussion below, in Section 5.3). Badly sorted glauconites are therefore more fragile than those that are well sorted.

The elemental analyses (Table 2) show that the major elements have a homogeneous distribution for all the samples studied. In particular, the K_2O and iron contents are relatively high and indicate that the glauconites can be qualified as mature (or evolved) or very mature (highly evolved), according to the pioneering work of Odin and Matter [1981]. With K_2O concentrations exceeding 8% of the glauconite composition in many samples, the mineral can be said to be highly evolved, which implies that its evolution

may have lasted between 100 ky and 1 My, according to Odin and Matter [1981]. The other samples analysed have K_2O content above 6.8% (evolved glauconite). Trace elements show more contrasting distributions. The chalk samples contain more Co and Ni than those of the Aptian-Albian sandstones and the Jurassic samples. In contrast, the Jurassic and Aptian-Albian samples are all enriched in As, Ge, V and Zn compared to the chalk samples. Among the elements sensitive to redox conditions, while vanadium is enriched, uranium is not and molybdenum is below the detection limit in most samples. Finally, the distribution of rare earth element (REE) shows that little difference is observed in the REE patterns from one sample to another (Supplementary Figure S9). An europium anomaly can be observed on each REE pattern. Thus, REE patterns are not a discriminating factor in the present study.

5. Interpretations

5.1. *Synsedimentary versus reworked glauconite*

We are faced with two contrasting logics, depending on whether we consider the glauconites present in the chalk of the Cenomanian or those present in the sandstones of the Aptian-Albian or in the Jurassic deposits. Previous work [Amorosi and Centineo, 2000, Tribovillard et al., 2021] showed that the glauconite of the Boulonnais chalk responded to the typical logic of formation: very slow sedimentation rate in the "Chalk Sea" in connection with the great transgression of the Upper Cretaceous, prolonged exchanges with seawater at the sediment–water interface, formation of a synsedimentary glauconite rich in iron and potassium, showing relatively large grains and an absence of particle size sorting. The long duration of the exchanges between the seawater and the sediment–water interface could have been caused by the reduced flux of particles or by winnowing induced by currents affecting the seabed [Giresse, 1985, Giresse et al., 2021, see the works of and references therein]. In contrast, the glauconite of the Aptian-Albian sandstones and that of most of the Jurassic deposits studied here show smaller, well sorted grains, which are therefore not synsedimentary but reworked from their source zones. Glauconite being a relatively dense mineral (d = 2.40–2.95 g/cm^3, most often 2.68 g/cm^3), it cannot be assumed that the grains were brought up from deeper or more distal zones by ascending marine currents. More probably, the glauconite grains must have been reworked from more proximal source zones with an emplacement linked to the hydrodynamics of the depositional environment [Huggett et al., 2017]. There is, however, a Jurassic facies in which the glauconite grains are not reworked: the oyster reefs observed at Cap Gris Nez and Cran du Noirda at the base of the Argiles de Châtillon Fm. Again, the grains are of relatively large size and do not show particle size sorting (Figures 2 and 3). Many of them have the same morphology as that of the grains observed within the chalk [Tribovillard et al., 2021]. It makes sense to regard them as syndeposit, based on the same reasoning as that used for chalk glauconite.

5.2. *Oyster patch reefs, a glauconite factory?*

In the Jurassic deposits, the base of the Argiles de la Crèche Fm. corresponds to a transgression, with the transition from shoreface sandstones (Grès de la Crèche Fm.) to silty marl being gradually more clayey upward (Argiles de la Crèche Fm.). Yet, unlike the Cretaceous chalk transgression discussed above, the transgressive Jurassic deposits show no glauconite enrichment. Sparse grains of glauconite are present but in very low abundance. The carbonate-free fraction is made up of quartz and clay particles (Supplementary Figure S8) with the exclusion of determinable glauconite.

The same logic did not prevail for the chalk and for the Jurassic deposits; the conditions necessary for the formation of glauconite in significant quantities were not met during the episodes of transgression recorded by the lower part of the Argiles de la Crèche. The simplest hypothesis is that this detrital formation had a significantly higher sedimentation rate than that of the Cenomanian chalk, which prevented protracted exchanges between the sediment–water interface and seawater. On the other hand, glauconite is present in very large abundance in Jurassic facies rich in bivalve shells: levels P1 and P2 of the Bancs Jumeaux, some lumachels of the Argiles de Châtillon, the beds rich in shells of the Assises de Croï and finally, the oyster reefs at the base of the Argiles de Châtillon. This level rich in oyster reefs (the so-called Boundary bed) which marks the transition between the shoreface sandstones of the Grès de Châtil-

lon and the marly to shaly Argiles de Châtillon was studied by Hatem et al. [2016]. It is strongly impacted by the precipitation of diagenetic limestone. If we disregard it, we can make the same observation as that which was made herein above for the transition from the Grès de la Crèche to the Argiles de la Crèche: the transgression which caused the evolution of the deposits of sand to silty/clayey/shale deposits was not accompanied by syn-deposit glauconite formation.

Our results show that the glauconite of the oyster reefs at the base of the Argiles de Châtillon, whether at Cap Gris-Nez or Cran du Noirda, is clearly synsedimentary, whereas that of the other shell-rich facies is always reworked. This finding suggests that the reefs were the source of the glauconite. The glauconite formed or accumulated in the oyster reefs, and would have been mobilized at the same time as the shells during storms (or very strong currents), and redeposited in the tempestites (coquina beds) and comparable facies (such as the P1 and P2 levels or the shell-rich bed of the Assises de Croï). Associations between glauconite and oyster or lumachel reefs are mentioned in the literature [e.g., Cloud Jr., 1955, Curtis Jr., 1955, Gardner, 1957, Glenn et al., 1994, Videt, 2003, Gréselle, 2007].

Glauconite can form in living oyster reefs because the conditions conducive to its authigenic formation are met there:

(1) The presence of abundant organic matter (decaying biomass, or necromass, and fecal pellets) promotes the development of low oxygen conditions [Southwell et al., 2017]. These authors report that oysters can withstand conditions of low oxygenation but that then, the development of the reef is limited by a slowed larval recruitment. However, it is commonly observed that suboxic conditions develop locally in such reefs. Such weakly reducing conditions favor the formation of glauconite in which iron is present in the form of Fe^{2+} and Fe^{3+}. More strongly reducing conditions would favor the Fe^{2+} form and, in the presence of sulfide ions generated by the activity of sulfate-reducing bacteria, the precipitation of pyritewould be observed and not that of glauconite [Meunier and El Albani, 2007].

(2) As oyster reefs develop in coastal or estuarine environments, iron may be abundant enough not to be a factor limiting the formation of iron minerals [e.g., Mayer, 1982, Jilbert et al., 2018, Herzog et al., 2020]. In addition, today's oysters are naturally rich in iron [e.g., Le Gall, 1948]. If this were also true for Jurassic oysters, then reefs would have been an environment particularly favorable to the formation of glauconite. In addition, the upward growth of the reefs helps to combat burial and facilitates protracted exchanges with seawater, allowing time for glauconite to grow.

In lumachels, glauconite is present but in variable proportions, always lower than in oyster reefs. On the other hand, pyrite is very abundant there, not in the form of framboids but in that of cement binding the shells. The presence of this pyrite suggests that reducing conditions may have developed in the coquina beds in response to the activity of sulfate-reducing bacteria feeding on the necromass of the oysters or their excreta. The presence of iron possibly linked to oysters could have favored the formation of pyrite and the conditions must have been too reducing for glauconite to form. The ex-situ formation of glauconite trapped in the coquina beds is attested by the good grain size sorting of the green grains and their very small size, which show that they have been reworked (Figure 3). Additionally, recent work by Toshchakov et al. [2018] report that bacteria are able to reduce glauconite *in vitro*. It involves bacteria coupling hydrogenogenic CO oxidation with the reduction of Fe^{3+} minerals to ensure the production of metabolic energy [see also Shapkin et al., 2013, Zavarzina et al., 2016]. If this dissimilatory reduction of structural Fe^{3+} from glauconite can be observed on the time scale of laboratory analyses, this suggests that on the time scale of diagenetic phenomena, a partial destruction of glauconite may occur. This could contribute to explain the low presence of glauconite in the facies of Boulonnais which underwent the most reducing conditions. This would also explain why the glauconite grains in the coquina beds appear unusually small and corroded when viewed under a microscope (Figure 3).

5.3. *In vitro wear of glauconite grains*

Particle size analysis showed that some populations of glauconite grains released extremely fine fractions (micrometer scale) during measurement in the instrument (probable wear of the grains by the rapid current inside the measuring instrument). These are

the glauconite grains from the facies where this mineral was formed authigenically (syndeposit: chalk, oyster reefs). On the other hand, the grains from reworked deposits (coquina beds, Assises de Croï, Aptian-Albian sands) do not show this release of micrometer-sized particles. This observation suggests that the reworked grains are more mechanically resistant than the other, as if the reworked grains had already lost their more fragile cortex. However, there are a few exceptions: some samples with well-sorted glauconite show the presence of the clay-sized fraction of glauconite (Figure 4 and Supplementary Figure S7).

5.4. *Redox proxy enrichments*

A difference is observed in the content of elements sensitive to redox conditions between the chalk samples and those of the other deposits (sandstones of the middle part of the Cretaceous, Jurassic deposits). The Cenomanian Chalk samples show a relatively high content of As and V, but not of U or Mo, as detailed by Tribovillard et al. [2021]. The present study confirms these results and shows that the samples other than those of the chalk are even richer in As and V while are not enriched U and Mo. The absence of enrichment in U and Mo in minerals that however formed under slightly reducing conditions is explained by the absence of mineralogical support from glauconite (for U and for Mo) and the limitation of sulfide ions that restricts the capture of Mo [Tribovillard et al., 2021]. On the other hand, V [which is a well-studied redox tracer; e.g., Breit and Wanty, 1991, Wanty and Goldhaber, 1992, Huang et al., 2015, Bian et al., 2022] is known to be easily incorporated into phyllosilicates during diagenesis/authigenesis phases [e.g., Gustafsson, 2019, Bennett and Canfield, 2020, and references therein], and As is known for its affinity for iron [Tribovillard, 2020]. However, as we know, glauconite is an iron-rich phyllosilicate. The presence of As and V is therefore expected, since glauconite forms under slightly reducing conditions. Moreover, these two elements can be transferred from the water column to the sediment in the form of organo-metallic complexes, the abundance of organic matter therefore impacts the distribution of these two elements in the sediments [Tribovillard et al., 2006, Tribovillard, 2020, Gustafsson, 2019, Algeo and Liu, 2020, Bian et al., 2022]. If the idea that the oyster reefs were the source zone of the glauconite of the Jurassic deposits of the Boulonnais is adopted, then their enrichments in As and V, significantly higher than those of the chalk samples, would reflect that the environmental conditions were more reducing and/or richer in organic matter in the close environment of oyster reefs than at the time of the chalk accumulation. This interpretation is reinforced by the distribution of germanium, a trace element substituting for silicium in silicates, and showing some redox-dependent behavior [Tribovillard et al., 2011]. The comparatively higher Ge enrichment in the Jurassic glauconite is consistent with the interpretation derived above using V and As.

If this result seems logical, it nevertheless shows that the elemental composition of glauconite can be used to reconstruct the redox conditions accompanying authigenesis/diagenesis. In this case, this reasoning can be applied to the glauconite present in very large quantities in the sandstones of the Aptian-Albian at the base of the chalk. This remarkably well-sorted glauconite was emplaced at the same time as the quartz grains of this detrital facies. These two phases are therefore reworked from more proximal zones on the occasion of the initiation of the great transgression of the Upper Cretaceous. This great transgression followed the emersion of the Boulonnais [and more broadly of the whole region; Mansy et al., 2007] that started during the latest Jurassic [leading to the accumulation of the Purbeckian facies; Mansy et al., 2007]. The resumption of marine sedimentation (mid-Cretaceous) induced by the return of the sea was therefore accompanied by the reworking of glauconite from more coastal zones, even estuaries, where the depositional conditions were to be confined. This confinement is attested by the high values of As, V and Ge contents, these values being the highest among those reported in the present study.

5.5. *Europium anomaly*

According to Jarrar et al. [2000], the negative europium (Eu) anomaly, commonly observed for glauconite, is presumably inherited from the source material, that is, the substrate upon which the authigenic growth of glauconite took place. The Eu anomaly reflects the deficiency of this element in the Earth's upper crust, because Eu values low enough to

induce europium reduction in sedimentary milieus is seldom observed [Bau and Möller, 1991]. The REE of glauconites are supplied by lithogenous, clastic material, and the contribution of seawater can be considered to be minimum [Fleet et al., 1980].

6. Conclusion

This work illustrates the diversity of the places where glauconite can form. In the Boulonnais, glauconite is formed in relatively deep environments (the bottom of the Cenomanian Chalk Sea), also formed (or was accumulated) within sparse oyster patch reefs of Jurassic age, and the Aptian-Albian sandstones, linked to an incipient major transgression, collected glauconite probably originating from shallow (estuarine?) environments.

In this work, the emphasis is set upon oyster patch reefs as sites of production of glauconite. The break up of such reefs during storms allowed glauconite to be exported downdip basinward together with shells, accumulating in noticeable proportions in coquina beds or shell-rich beds.

Comparing glauconites formed in contrasting environments teaches us that their V, As and Ge concentrations are a tool for assessing the redox conditions prevailing during authigenesis, in milieus where these conditions were mildly reducing. As a matter of fact, strongly reducing environments favor pyrite precipitation over, or at the expense of, glauconite: in such environments, it may be put forward that glauconite could be (partly) destroyed post-deposition.

Conflicts of interest

Authors have no conflict of interest to declare.

Acknowledgements

We thank Olivier Averbuch, Jean-François Deconinck, François Guillot and Alain Trentesaux for sharing their knowledge of the geology of Boulonnais, as well as the reviewers and the CR Geoscience team, who helped make things possible and better than they were initially. We are grateful to Monique Gentric for her administrative management of the project. Our thanks to undergraduate intern Cynthia Richard. This project received financial support from the INSU Tellus Syster program. We sincerely thanks the Earth Science Department of University of Lille for its support.

Supplementary data

Supporting information for this article is available on the journal's website under https://doi.org/10.5802/crgeos.170 or from the author.

References

Algeo, T. J. and Liu, J. (2020). A re-assessment of elemental proxies for paleoredox analysis. *Chem. Geol.*, 540, article no. 119549.

Amorosi, A. (1995). Glaucony and sequence stratigraphy: a conceptual framework of distribution in siliciclastic sequences. *J. Sediment. Res.*, B65, 419–425.

Amorosi, A. and Centineo, M. C. (2000). Anatomy of a condensed section: the lower cenomanian glaucony-rich deposits of cap Blanc-Nez (Boulonnais, Northern France). In Glenn, C. R., Prevot-Lucas, L., and Lucas, J., editors, *Marine Authigenesis: From Global to Microbial*. SEPM Society for Sedimentary Geology, Tulsa, OK.

Baldermann, A., Banerjee, S., Czuppon, G., Dietzel, M., Farkaš, J., Löhr, S., Moser, U., Scheiblhofer, E., Wright, N. M., and Zack, T. (2022). Impact of green clay authigenesis on element sequestration in marine settings. *Nat. Commun.*, 13, article no. 1527.

Banerjee, S., Bansal, U., Pande, K., and Meena, S. S. (2016a). Compositional variability of glauconites within the upper cretaceous karai shale formation, Cauvery Basin, India: implications for evaluation of stratigraphic condensation. *Sediment. Geol.*, 331, 12–29.

Banerjee, S., Bansal, U., and Thorat, U. V. (2016b). A review on palaeogeographic implications and temporal variation in glaucony composition. *J. Palaeogeogr.*, 5, 43–71.

Banerjee, S., Chakrabarty, S., Choudhury, T. R., et al. (2022). The application of glauconite for high-resolution stratigraphic interpretations of eocene succession. In Meghraoui, M. et al., editors, *Advances in Geophysics, Tectonics and Petroleum Geosciences. CAJG 2019*, Advances in Science, Technology & Innovation. Springer, Cham.

Banerjee, S., Jeevankumar, S., and Eriksson, P. G. (2008). Mg-rich ferric illite in marine transgressive and highstand systems tracts: examples from the Paleoproterozoic Semri Group, central India. *Precambrian Res.*, 162, 212–226.

Bau, M. and Möller, P. (1991). Rare earth element fractionation in metamorphogenic hydrothermal calcite, magnesite and siderite. *Mineral. Petrol.*, 45, 231–246.

Bayliss, P. and Syvitski, J. P. M. (1982). Clay diagenesis in recent marine fecal pellets. *Geo-Marine Lett.*, 2, 83–88.

Bennett, W. W. and Canfield, D. E. (2020). Redox-sensitive trace metals as paleoredox proxies: A review and analysis of data from modern sediments. *Earth-Sci. Rev.*, 204, article no. 103175.

Bian, B., Chappaz, A., Schovsbo, N. H., and Sanei, H. (2022). A new vanadium species in black shales: Updated burial pathways and implications. *Geochim. Cosmochim. Acta*, 338, 1–10.

Bout-Roumazeilles, V., Cortijo, E., Labeyrie, L., and Debrabant, P. (1999). Clay-mineral evidence of nepheloid layer contribution to the Heinrich layers in the Northwest Atlantic. *Palaeogeogr. Palaeoclimatol. Palaeoecol.*, 146, 211–228.

Boyer, P. S., Guinness, E. A., Lynch-Blosse, M. A., and Stolzman, R. A. (1977). Greensand fecal pellets from New Jersey. *J. Sediment. Res.*, 4, 267–280.

Breit, G. N. and Wanty, R. B. (1991). Vanadium accumulation in carbonaceous rocks: a review of geochemical controls during deposition and diagenesis. *Chem. Geol.*, 91, 83–97.

Carignan, J., Hild, P., Morel, J., and Yeghicheyan, D. (2004). Routine analysis of trace elements in geochemical samples using flow injection and low-pressure on-line liquid chromatography coupled to ICP-MS: a study of geochemical references materials BR, DR–N, UB–N, AN–G and GH. *Geostand. Newslett.*, 25, 187–198.

Chamley, H. (2001). Clay mineralogy. In *Encyclopedia of Ocean Sciences*, pages 462–471. Elsevier, Amsterdam.

Choudhury, T. R., Banerjee, S., Khanolkar, S., Saraswati, P. K., and Meena, S. S. (2021). Glauconite authigenesis during the onset of the Paleocene-Eocene thermal maximum: A case study from the Khuiala Formation in Jaisalmer Basin, India. *Palaeogeogr. Palaeoclimatol. Palaeoecol.*, 571, article no. 110388.

Cloud Jr., P. E. (1955). Physical limits of glauconite formation. *Bull. Amer. Assoc. Petrol. Geol.*, 39, 484–492.

Curtis Jr., N. M. (1955). Paleoecology of the viesca member of the weches formation at Smithville, Texas. *J. Paleontol.*, 29, 263–282.

El Albani, A., Meunier, A., and Fursich, F. (2005). Unusual occurrence of glauconite in a shallow lagoonal environment (Lower Cretaceous, northern Aquitaine Basin, SW France). *Terra Nova*, 17, 537–544.

Fleet, A. J., Buckley, H. A., and Johnson, L. R. (1980). The rare earth element geochemistry of glauconites and celadonites. *J. Geol. Soc. London*, 137, 683–688.

Fürsich, F. and Oschmann, W. (1986). Storm shell beds of Nanogyra virgula in the upper Jurassic of France. *Neues Jahrb. Geol. Palaontol. Abh.*, 172, 141–161.

Gardner, J. (1957). Little Stave Creek, Alabama – Paleoecologic study. In *Geological Society of America Memoir 67*. Geological Society of America, Boulder, Colorado. Chapter 20.

Giresse, P. (1985). Le fer et les glauconies au large de l'embouchure du fleuve Congo. *Sci. Géol., Bull.*, 38, 293–322.

Giresse, P., Bayon, G., Tallobre, C., and Loncke, L. (2021). Neodymium isotopes in glauconite for palaeoceanographic reconstructions at continental margins: a preliminary investigation from Demerara Rise. *Front. Earth Sci.*, 9, article no. 652501.

Glenn, C. R., Arthur, M. A., Resig, J. M., Burnett, W. C., Dean, W. E., and Jahnke, R. A. (1994). Are modern and ancient phosphorites really so different? In Iijima, A., Abed, A. M., and Garrison, R. E., editors, *Siliceous, Phosphatic and Glauconitic Sediments of the Tertiary and Mesozoic*, pages 159–188. VSP Sci. Publ., Zeist.

Gréselle, B. (2007). *Impact des variations paléoclimatiques sur la sédimentation carbonatee au Valanginien*. PhD thesis, Université Claude Bernard, Lyon I. Minéralogie. tel-00275099.

Gustafsson, J. P. (2019). Vanadium geochemistry in the biogeosphere – speciation, solid-solution interactions, and ecotoxicity. *Appl. Geochem.*, 102, 1–25.

Hatem, E., Tribovillard, N., Averbuch, O., Sansjofre, P., Adatte, T., Guillot, F., Ader, M., and Vidier, D. (2016). Early diagenetic formation

of carbonates in a clastic-dominated ramp environment impacted by synsedimentary faulting-induced fluid seepage - Evidence from the Late Jurassic Boulonnais Basin (N France). *Mar. Pet. Geol.*, 72C, 12–29.

Hatem, E., Tribovillard, N., Averbuch, O., Vidier, D., Sansjofre, P., Birgel, D., and Guillot, F. (2014). Oyster patch reefs as indicators of fossil hydrocarbon seeps induced by synsedimentary faults. *Mar. Pet. Geol.*, 55, 176–185.

Herzog, S. D., Persson, P., Kvashnina, K., and Kritzberg, E. S. (2020). Organic iron complexes enhance iron transport capacity along estuarine salinity gradients of Baltic estuaries. *Biogeosciences*, 17, 331–344.

Hesselbo, S. P. and Huggett, J. (2001). Glaucony in ocean-margin sequence stratigraphy (Oligocene-Pliocene, Offshore New Jersey, USA; ODP Leg 174A). *J. Sediment. Res.*, 71, 599–607.

Huang, J. H., Huang, F., Evans, L., and Glasauer, S. (2015). Vanadium: global (bio)geochemistry. *Chem. Geol.*, 417, 68–89.

Huggett, J., Adetunji, J., Longstaffe, F., and Wray, D. (2017). Mineralogical and geochemical characterisation of warm-water, shallow-marine glaucony from the Tertiary of the London Basin. *Clay Miner.*, 52, 25–50.

Huggett, J. M. (2021). Glauconites. In *Encyclopedia of Geology*, pages 334–340. Elsevier, Amsterdam, 2nd edition.

Jarrar, G., Amireh, B., and Zachmann, D. (2000). The major, trace and rare earth element geochemistry of glauconites from the early Cretaceous Kurnub Group of Jordan. *Geochem. J.*, 34, 207–222.

Jilbert, T., Asmala, E., Schröder, C., Tiihonen, R., Myllykangas, J. P., Virtasalo, A., Kotilainen, J. J., Peltola, P., Ekholm, P., and Hietanen, S. (2018). Impacts of flocculation on the distribution and diagenesis of iron in boreal estuarine sediments. *Biogeosciences*, 15, 1243–1271.

Le Gall, J. V. (1948). *Valeur Nutritive et Valeur Thérapeutique de L'huitre*, volume 2 of *Notes et Rapports de l'Office Scientifique et Technique des pêches maritimes, Nouvelle Série*. Office Scientifique et Technique des Pêches Maritimes.

López-Quirós, A., Sánchez-Navas, A., Nieto, F., and Escutia, C. (2020). New insights into the nature of glauconite. *Am. Mineral.*, 105, 674–686.

Mansy, J.-L., Guennoc, P., Robaszynski, F., Amédro, F., Auffret, J.-P., Vidier, J.-P., Lamarche, J., Lef, D., Sommé, J., Brice, D., Mistiaen, B., Prud'homme, A., Rohart, J.-C., and Vachard, D. (2007). *Notice Explicative, Carte Géologique de la France (1/50 000), Feuille Marquise*. BRGM, Orléans, 2nd edition.

Mayer, L. M. (1982). Retention of riverine iron in estuaries. *Geochim. Cosmochim. Acta*, 46, 1003–1009.

Meunier, A. and El Albani, A. (2007). The glauconite–Fe-illite–Fe-smectite problem: a critical review. *Terra Nova*, 19, 95–104.

Odin, G. S. and Matter, A. (1981). De glauconiarum origine. *Sedimentology*, 28, 611–641.

Shapkin, A. A., Chistyakova, N. I., Rusakov, V. S., Zhilina, T. N., and Zavarzina, D. G. (2013). Mössbauer study of bacterial iron-reduction processes in natural glauconite and biotite. *Bull. Russ. Acad. Phys.*, 77, 734–738.

Southwell, M. W., Veenstra, J. J., Adams, C. D., Scarlett, E. V., and Payne, K. B. (2017). Changes in sediment characteristics upon oyster reef restoration, NE Florida, USA. *J. Coast. Zone Manag.*, 20, article no. 442.

Toshchakov, S. V., Lebedinsky, A. V., Sokolova, T. G., Zavarzina, D. G., Korzhenkov, A. A., Teplyuk, A. V., Chistyakova, N. I., Rusakov, V. S., Bonch-Osmolovskaya, E. A., Kublanov, I. V., and Gavrilov, S. N. (2018). Genomic insights into energy metabolism of Carboxydocella thermautotrophica coupling hydrogenogenic CO oxidation with the reduction of Fe(III) Minerals. *Front. Microbiol.*, 9, article no. 1759.

Trentesaux, A., Recourt, P., Bout-Roumazeilles, V., and Tribovillard, N. (2001). Carbonate grain-size distribution in hemipelagic sediments from a laser particle sizer. *J. Sediment. Res.*, 71, 858–862.

Tribovillard, N. (2020). Arsenic in marine sediments: how robust a redox proxy? *Palaeogeogr. Palaeoclimatol. Palaeoecol.*, 550, article no. 109745.

Tribovillard, N., Algeo, T. J., Lyons, T. W., and Riboulleau, A. (2006). Trace metals as paleoredox and paleoproductivity proxies: An update. *Chem. Geol.*, 232, 12–32.

Tribovillard, N., Bout-Roumazeilles, V., Delattre, M., Ventalon, S., Abraham, R., and Nzié, O. (2021). Syndepositional glauconite as a paleoenvironmental proxy – the lower Cenomanian Chalk of Cap Blanc Nez (N-France). *Chem. Geol.*, 584, article no. 120508.

Tribovillard, N., Bout-Roumazeilles, V., Riboulleau, A., Baudin, F., Danelian, T., and Riquier, L. (2011). Transfer of germanium to marine sediments: Insights from its accumulation in radiolarites and authigenic capture under reducing conditions. Some examples through geological ages. *Chem. Geol.*, 282, 120–130.

Tribovillard, N., Sansjofre, P., Ader, M., Trentesaux, A., Averbuch, O., and Barbecot, F. (2012). Early diagenetic carbonate bed formation at the sediment-water interface triggered by synsedimentary faults. *Chem. Geol.*, 300/301, 1–13.

Velde, B. (2014). Sediments, diagenesis and sedimentary rocks. In *Treatise Geochemistry*, volume 9, pages 351–364. Elsevier, Amsterdam, 2nd edition.

Videt, B. (2003). *Dynamique des paléoenvironnements à huîtres du Crétacé Supérieur nord-aquitain (SO France) et du Mio-Pliocène andalou (SE Espagne): biodiversite, analyse séquentielle, biogéochimie*. PhD thesis, Université Rennes 1. tel-00006038.

Wanty, R. B. and Goldhaber, M. B. (1992). Thermodynamics and kinetics of reactions involving vanadium in natural systems: Accumulation of vanadium in sedimentary rocks. *Geochim. Cosmochim. Acta*, 56, 1471–1483.

Zavarzina, D. G., Chistyakova, N. I., Shapkin, A. V., Savenko, A. V., Zhilina, T. N., Kevbrin, V. V., Alekseeva, T. V., Mardanov, A. V., Gavrilov, S. N., and Bychkov, A. Yu. (2016). Oxidative biotransformation of biotite and glauconite by alkaliphilic anaerobes: The effect of Fe oxidation on the weathering of phyllosilicates. *Chem. Geol.*, 439, 98–109.